Nanoscale

PAPER

View Article Online
View Journal

Cite this: DOI: 10.1039/d0nr08762a

Segregation-controlled self-assembly of silver nanowire networks using a template-free solution-based process†

Ji Won Shin,‡[a] Hyo-Ryoung Lim,‡[b] Hong-Baek Cho, *[a] Young-Tae Kwon[c] and Yong-Ho Choa *[a]

Metal conductive patterning has been studied as an alternative to the most commonly used indium tin oxide electrodes. Printed electrodes are fabricated by several complicated processes including etching, photolithography, and laser- and template-based techniques. However, these patterning methods have increasingly encountered critical issues of long manufacturing times and high equipment costs that necessitate vacuum and high-temperature conditions. In this study, we present a template-free solution-based patterning method for the fabrication of transparent electronics by inducing segregation-based networks of silver nanowires (SGAgNWs); this is a potential method to fabricate cost effective and scalable optoelectronics. Micro-dimensional fine-patterned segregated networks with conductive cells are created by the self-assembly of one-dimensional nanomaterials under optimal ink conditions wherein different types of solvents and aspect ratios of silver nanowires (AgNWs) are formulated. Photoelectric properties can be controlled by adjusting the size of the cell, which is an empty domain surrounded by the AgNW assembly with microscale cell-to-cell distance dimensions ranging between 4 to 345 μm. The as-obtained AgNW metal grid—formulated on a polyethylene terephthalate film—was identified as a high-performance transparent electrode (TE) device with excellent optoelectronic properties of 87.08% transmittance and 50 Ω □$^{-1}$ resistance. In addition, the electrical conductivity of the TE film is enhanced with a very low haze of less than 4% because of the intense pulsed light treatment that diminished the sheet resistance to 21.36 Ω □$^{-1}$, which is attributed to the creation of welded silver networks. The SGAgNW concept for TE technology demonstrates a very promising potential for use in next-generation flexible electronic devices.

Received 10th December 2020,
Accepted 5th April 2021

DOI: 10.1039/d0nr08762a

rsc.li/nanoscale

Introduction

Transparent electrodes (TEs) are transparent to visible light, yet they are electrically conductive; they are a necessary component in several research fields including optoelectronic devices, touch screens, smart windows, solar cells, and heaters of microchips and sensors.[1–3] It is important to select conducting materials suitable for transparent electronic devices. To this end, various types of materials have been studied; metal oxides, such as tin-doped indium oxide (ITO) and fluorine-doped tin oxide (FTO), are commonly used.[4] However, the use of such oxide-based conventional rigid electronics has critical limitations owing to their fragile ceramic nature, scarcity of indium, high processing temperatures, and lack of applications in flexible electronics.[5] Thus, recent studies have focused on next-generation material metal conductive patterns for the replacement of ITO.

Metal-based nanostructures with flexible properties have been promising TE candidates owing to their excellent characteristics, such as stretchability, bendability, foldability, and lightweightness.[6,7] They have a wide range of applications in the semiconductor industry, such as flexible displays, smart windows, touch screens, flexible solar cells, flexible transparent heater auto-mobile window defrosters, and outdoor panel displays.[8,9] Among metallic materials, AgNWs are advantageous because of their relatively simple synthesis that utilizes low-cost and large-scale manufacturing methods, such as the polyol process.[10] Furthermore, their electrical, optical, and

[a]Department of Materials Science and Chemical Engineering, Hanyang University, Ansan 15588, South Korea
[b]George W. Woodruff School of Mechanical Engineering, Institute for Electronics and Nanotechnology, Georgia Institute of Technology, Atlanta, GA 30332, USA. E-mail: choa15@hanyang.ac.kr, hongbaek@hanyang.ac.kr
[c]Metal Powder Department, Korea Institute of Materials Science, Changwon, 51508, Republic of Korea

†Electronic supplementary information (ESI) available. See DOI: 10.1039/d0nr08762a

‡These authors contributed equally to this work.

mechanical properties are comparable to those of ITO; among metals, silver has the lowest residual resistivity of 1.62×10^{-7} Ω m, a high corrosion resistance, and superior flexibility and stability.[10–12] AgNW patterns have been widely fabricated in metal grids of TEs by using lithography, etching, nanoimprinting, and transfer stamping.[13–15] Despite the advantages of printing, it has been proven challenging to fabricate a transparent conductive mesh of such metal nanowires without employing high-cost equipment that requires high-vacuum conditions and high-resolution light sources, as described in several published methods.[16,17]

In this study, we introduce a new patterning process that creates highly transparent, conductive, and percolated metallic networks that comprise microscale arrays of cell-shaped AgNW meshes *via* the self-assembly of colloidal silver inks (Fig. 1). The method depends on interactions between a couple of solvents and the self-assembling AgNWs influenced by the aspect ratio of the AgNWs, the combination of solvents, differences in viscosity, boiling point, and density, and the thermal treatment employed after film casting. Compared with the processes in other studies, wherein meshes are formed in multiple steps, it is possible to use a one-step process to control the settings of the evaporation temperature of each solvent and to create novel segregation-based networks of silver nanowires (SGAgNW).

We systematically varied the aspect ratios and concentrations of AgNWs to control the TE performance, and we studied the resulting morphologies of the tuned silver net-

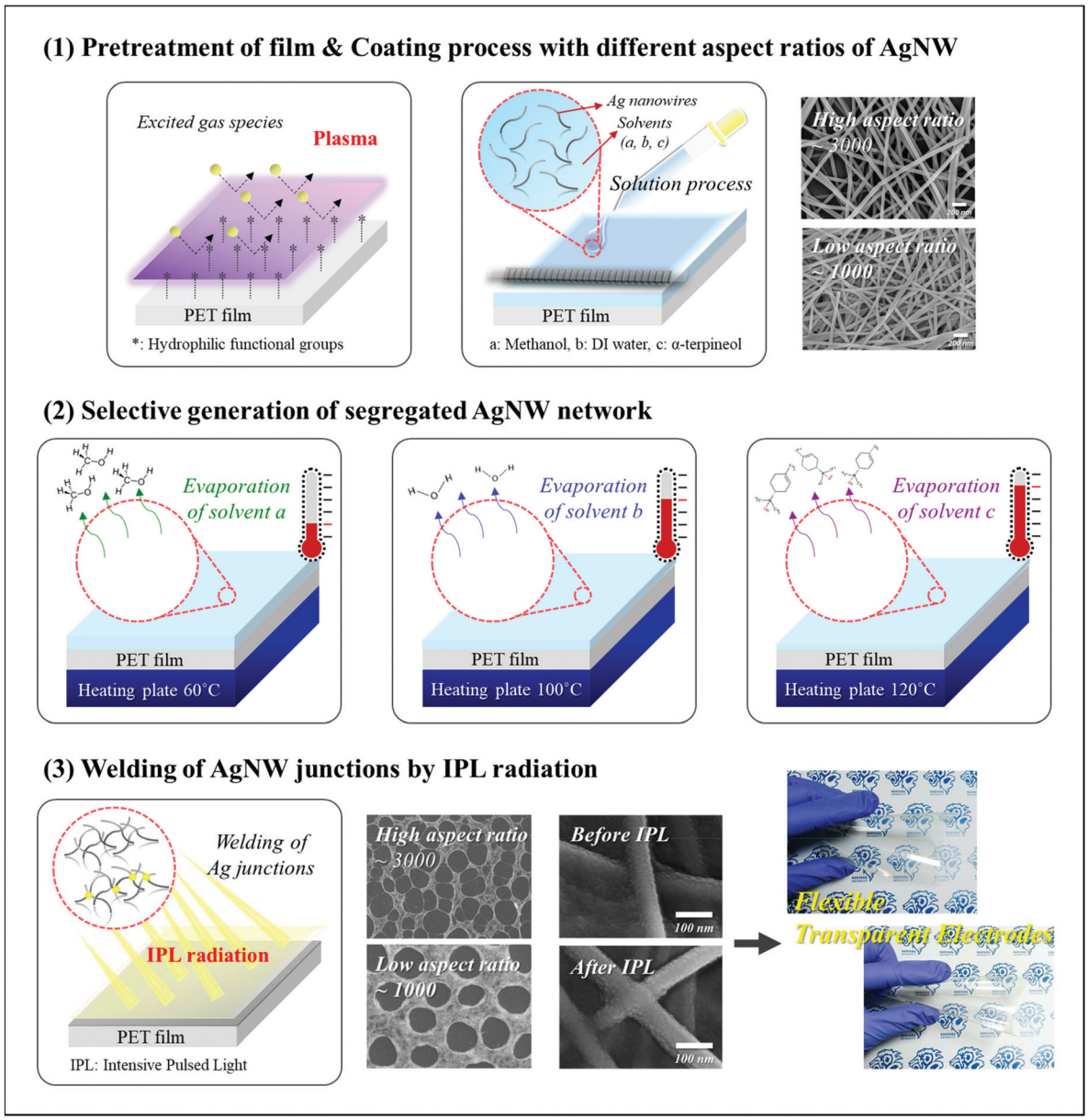

Fig. 1 Schematic of the experimental procedure for fabricating AgNW patterned transparent thin films.

works. It is demonstrated that the tuned properties of solutions lead to the arrangement of arrays of nanowires into cell shapes, without preparing a template and forming a mesh frame separately. Thermal sintering is used to enhance conductivity of metal powders by removing organic ligands. However, thermal sintering induces large power dissipation and unwanted deformation of the polymer substrates. In this study, an intense pulsed light (IPL) sintering approach is employed to create a connection of Ag nanowire junctions for an added reduction in sheet resistance. The silver NW segregated filler morphology formed cell-shaped continuous networks with open areas that contribute to the high transparency. Furthermore, the connected NW filler assembly provides excellent electrical conductivity on a robust and flexible substrate.

Experimental

Materials

Methanol (MeOH, 99.5%, Daejung Chemicals & Metals Co., Ltd, Korea), ethanol (EtOH, 99.9%, Daejung Chemicals & Metals Co., Ltd, Korea), and α-terpineol (>80.0%, Tokyo Chemical Industry Co., Ltd, Japan) were utilized as raw materials. Deionized (DI) water with a resistivity of 18.3 MΩ cm was used after treatment by a reverse-osmosis water filtration system (RO 2000, Nexpure®). A polyethylene terephthalate film (PET, XG532, Toray Saehan Inc., Korea), with a thickness of 125 μm, was used after sonication in EtOH and DI water for 10 min. Aqueous AgNW solutions with high (2.0 wt%, ACS materials, USA) and low aspect ratios (0.5 wt%, NanoPyxis Co., Ltd, Korea) were used after dispersion in DI water. For AgNWs with a high aspect ratio, the length/diameter (L/D) ratio is ~3000 with a broad distribution for an average diameter of 45.6 ± 4.4 nm and a length of 150 μm_{av} (Fig. S1a and b†). AgNWs with a low aspect ratio have a thin diameter of 43.3 ± 2.8 nm and length of 30 μm_{av} with an L/D ratio around 1000 and a relatively narrower distribution (Fig. S1c and d†). The crystalline structures of the high- and low-aspect-ratio AgNWs were confirmed by XRD, as shown in Fig. S2.† In the range of 20–90° (2 theta), the diffraction peaks are indexed to the face-centered cubic structure of Ag (JCPDS no. 03-065-2871).[18] The major peaks are located at 2 theta = 38.2° (111), 44.3° (200), 64.4° (220), 77.4° (311) and 81.5° (222), with no additional peaks. All nanowires exhibited high intensity at the (111) plane, indicating the preferred crystallographic orientation.[19] The longer AgNW is more than three times longer than the shorter one, as described in the Experimental section.

Preparation of AgNW coating ink

The coating ink was composed of methanol, α-terpineol, and an AgNW solution. The AgNW dispersion was washed with DI water by centrifugation at 8000 rpm for 5 min and was then formulated into a coating ink by using silver nanowires with two different aspect ratios: a high aspect ratio (2.0 wt% of AgNWs from ACS materials) and low aspect ratio (0.5 wt% of AgNWs from NanoPyxis Co., Ltd). The concentrations of AgNWs in the same amount of solution were controlled as follows: 0.25, 0.5, 1.0, 2.0, and 3.0 wt%. A silver ink solution with a high aspect ratio was formulated at a fixed ratio of methanol (5.0 g), α-terpineol (2.5 g), and 2.5 g of the AgNW solution. The weight fraction of the methanol and α-terpineol in a silver ink containing the low aspect ratio was modified to a ratio of 6 : 1.5 to control the degree of dilution. The ink solution was then stirred for 1 min and sonicated for 30 s.

Fabrication of self-assembled AgNW network patterns

A PET film (12 cm × 12 cm) underwent oxygen plasma treatment for 10 s using a reactive ion etching plasma system (ICP-PIE, Standard Asher RIE System, SNTEK Co., Ltd, Korea) to create hydrophilic groups on the surface. The formulated ink was coated on the PET film using a Meyer rod bar (#22, RD specialties, USA), and the film was then dried on a hot plate at 70 °C. The segregated AgNW pattern was annealed at 135 °C for 2 h; it was then sintered by an intense pulsed light (IPL) sintering technique (IPL-45kW_2100, PSTEK Co., Ltd, Korea) to enhance the TE performance. IPL technique from a xenon lamp excites plasmon resonance induced heating leading to fast sintering of metal nanowires under ambient conditions within seconds, and without damaging the substrate such as polymer film.[20–22] The stepwise process for fabricating flexible TE films is shown in Fig. 1.

SGAgNW-based thin film for TE and heater applications

TE films coated with 0.1% and 0.2% AgNWs with a low aspect ratio were selected and employed for the heater application. The sample size was cut to 7 cm × 9 cm. The sample films were connected to a DC power supply (SDP30-10D, SM Techno, Korea) and an ammeter to measure the current and voltage data. The operating voltages were applied to the heaters at input voltages of 3–10 V; the heating performance was measured using a temperature probe (TP-04, Lutron Electronic Enterprise Co., Ltd, Taiwan). The thermal stability was analyzed by a repeated test of five cycles at an input voltage of 7 V.

Characterization

The surface morphology was observed by optical microscopy (OM, KH-7700, Hirox Co Ltd) and field-emission scanning electron microscopy (FE-SEM, S-4800, Hitachi Ltd). The elemental composition was characterized using an X-ray energy dispersive spectrometer (EDS, EX-250, Horiba). The cell size and cell-to-cell distance were measured using the Image Tool program (UTHSCSA Image Tool for Windows version 3.0). The XRD pattern of the AgNWs was examined using an X-ray diffractometer (XRD, D/MAX-2500/PC, Rigaku) with Cu-Kα target irradiation (λ = 1.54 Å). The optical transmittance of the patterned film was obtained using a UV-visible spectrophotometer (Mega-2100, Scinco Co., Ltd) over the wavelength range of 400–750 nm, and the T(%) was selected at a wavelength of 550 nm. A PET film with 88.4% of transmittance was utilized as a reference; it was removed when determining the transmit-

tance value of the AgNW-coated PET films. The haze values were obtained using a haze meter (NDH-2000N, Nippon Denshoku Industries Co., Ltd). The sheet resistance (R_s) was measured using a four-point probe technique (CMT-SR2000N, AIT Co., Ltd) by averaging 10 measurements at different locations.

Results and discussion

Purified silver nanowires were obtained by repeated centrifugation, as described for the preparation of the AgNW coating ink. The images and diameter distributions of each of the long and short silver nanowires were obtained by SEM as shown in Fig. S1;† the morphology is described in the experimental section. In solution-based deposition, the surface treatment of substrates is critical for improving the adhesion between the coating material and substrate. The bare PET sample had a transparency of 88.4% and haze of 1.1% at 550 nm.[23] In addition to this high transparency, the thermal stability, chemical resistance, formability, and degree of hardness facilitate the use of PET in industry, whereas its hydrophobic nature is disadvantageous for adhesion, printing, and metallization.[24] Herein, an oxygen plasma treatment was performed for making the PET film surface more hydrophilic, as shown in Fig. S3.† The contact angle of the silver ink solution on the pristine PET was 72.83°, which was reduced to 38.27° after the oxygen plasma treatment on the PET surface, thereby confirming the enhanced wettability of the substrate. Plasma treatment produces polar groups, such as –OH, –COOH, and –C═O, on the surface, and it increases the surface roughness and hydrophilicity of the PET surface.[25] Therefore, it is believed that the hydrophobic PET film was modified with hydrophilic functional groups, facilitating the wettability of the silver ink. Morphological changes induced by AgNW distribution on the TE were investigated by controlling the distribution of AgNWs with different aspect ratios as a function of AgNW concentration. For comparing the effects of the two types of AgNWs, we fixed the amount of solvent to restrict the experimental parameters, adjusted the concentration of AgNWs from 0.1 to 3.5%, and observed the morphology by using SEM images, as shown in Fig. 2. Metal nanowire networks, comprising high- and low-aspect-ratio AgNWs, were assembled on a hydrophilic PET film with cell-shaped segregated patterns, formed by self-assembly during solvent evaporation after coating the silver ink. Open areas were located in the center of the pattern, and the nanowires accumulated on the edge like an array of rings. For a film formed by high-aspect-ratio AgNWs, the cell size of the segregation-based networks of silver nanowires (SGAgNWs) decreased gradually until the concentration of AgNWs reached 1.0 wt% and then became saturated. However, the cell structure is not formed when the concentration is too low, *i.e.*, at 0.1 wt%. In the case of the film formed by the low aspect ratio AgNWs, the cell size was reduced as the concentration of AgNWs was increased from 0.1 to 1.0%. At concentrations of 1.0% and higher, the surface was covered with nanowires because of the densely interconnected nanowires at concentrations of 2.0 and 3.5% (Fig. S4†). Comparing the two types of AgNWs, the nanowires with shorter lengths are assembled into a relatively spherical shape and they more effectively obtain a uniform SGAgNW pattern. At the same concentration of AgNWs, the distance between cells is estimated to be longer in the low-aspect-ratio silver-based networks because the number of nanowires in the solution is larger than that of long nanowires. That is, nanowires with lower aspect ratios are distributed more widely on

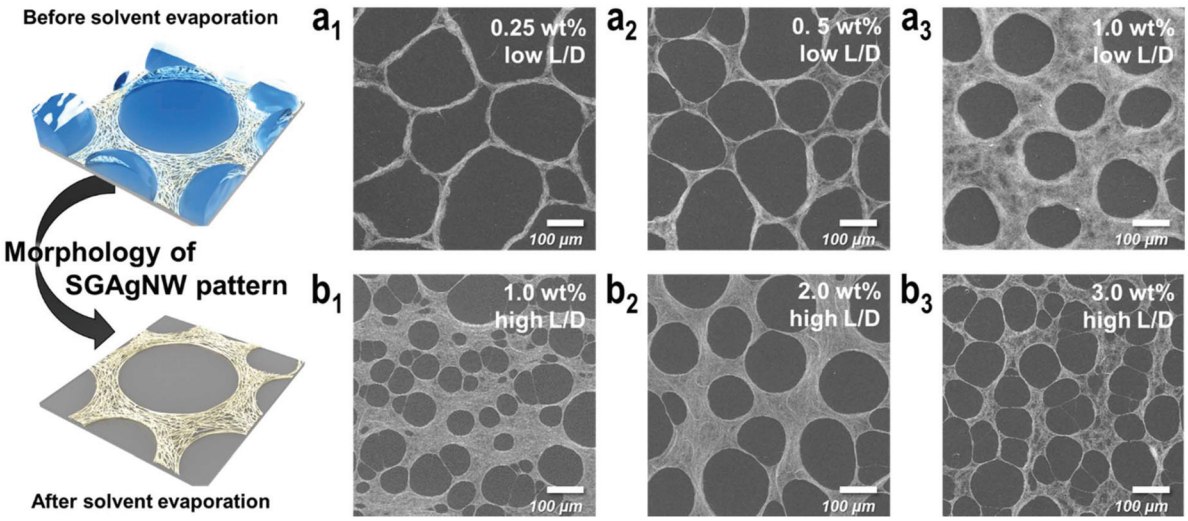

Fig. 2 Morphology of AgNW networks to fabricate transparent thin films. (a) SEM images of the self-assembled AgNWs for the low aspect ratio of (a_1) 0.25 wt%, (a_2) 0.5 wt%, and (a_3) 1.0 wt%. (b) SEM images of the self-assembled AgNWs for the high aspect ratio of (b_1) 1.0 wt%, (b_2) 2.0 wt%, and (b_3) 3.0 wt%.

the film surface. Thus, the cell-shaped pattern is competitive as a conducting film; it has high transparency because of the large number of open areas.

The effect of the aspect ratio of AgNWs on the formation of the cell shape was compared by analyzing the microstructure of the SGAgNW patterns using the ImageTool software. The distribution of the measured cell sizes and cell-to-cell distances are shown in Fig. 3. Both types of AgNWs showed a similar tendency until the nanowire concentration increased to 1.0 wt%, with a decrease in cell size and an increase in cell-to-cell distance as a function of Ag concentration; then, they showed a different trend only at higher concentrations. In the case of the low-aspect-ratio specimen, the coverage of the film surface became extremely high at concentrations exceeding 2.0 wt%; this is not appropriate for a TE because the low transparency makes it a dense thin film without open space (see also Fig. S4a4 and a5†). The cell size distribution was relatively regular at lower Ag concentrations with a narrow deviation in contrast to the high-aspect-ratio specimen. For the low aspect ratio NWs, the cell size was 145.38 μm and the cell-to-cell distance was 22.37 μm at 0.5 wt% AgNW concentration. When the concentration increased to 1.0 wt%, the cell size decreased slightly (126.08 μm) and the distance scale of the pattern increased up to ~70 μm. The cell morphology was optimized at 1.0 wt% for the short nanowires. In contrast, for the 2.0 wt% AgNWs with a high aspect ratio, an increase in cell size from 78.96 μm (1.0 wt%) to 84.41 μm was observed and the cell-to-cell distance also increased to 34.76 μm from 20.22 μm (1.0 wt%). The cell size and cell-to-cell distance further increased to 106.09 μm and 43.88 μm, respectively, at 3.0 wt% concentration of AgNWs. It is presumed that the larger the cell size, the better the enhancement of the transmittance. The cell-to-cell distance is related to the formation of the conduction network that reduces sheet resistance. Optimized conditions of the SGAgNW patterns are estimated in coordination with the resulting optical and electrical properties.

We evaluated the performance of the self-assembled patterns for comparing the optical and electrical properties of the two types of AgNWs. The optical transmittance spectrum in the visible region was recorded and is shown in Fig. 4(a and b). In the cell-shaped pattern with a low aspect ratio, the optical transmittance at 550 nm is high (>81%) at concentrations below 1.0 wt%; the transmittance is less than 75% at 2.0 wt% and 3.0 wt%, which correlates with the morphologies in the SEM images. However, for the high aspect ratio, the

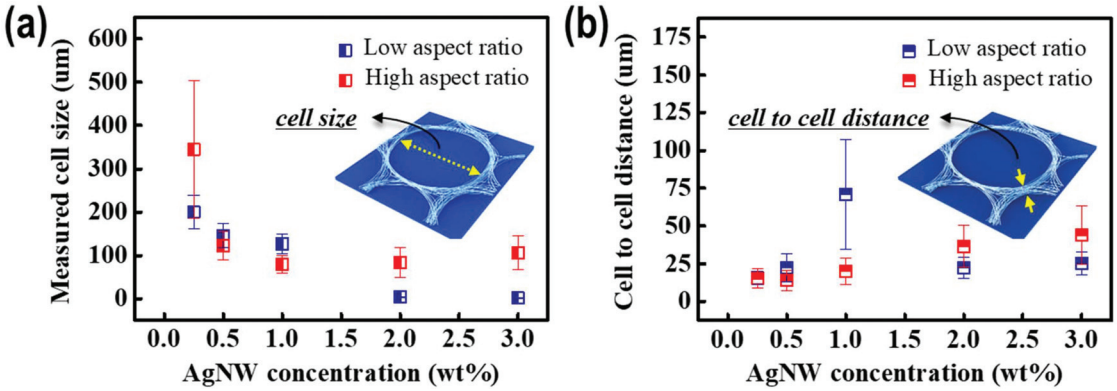

Fig. 3 Measured cell sizes and cell-to-cell distances of the self-assembled AgNWs. (a) Low aspect ratio and (b) high aspect ratio.

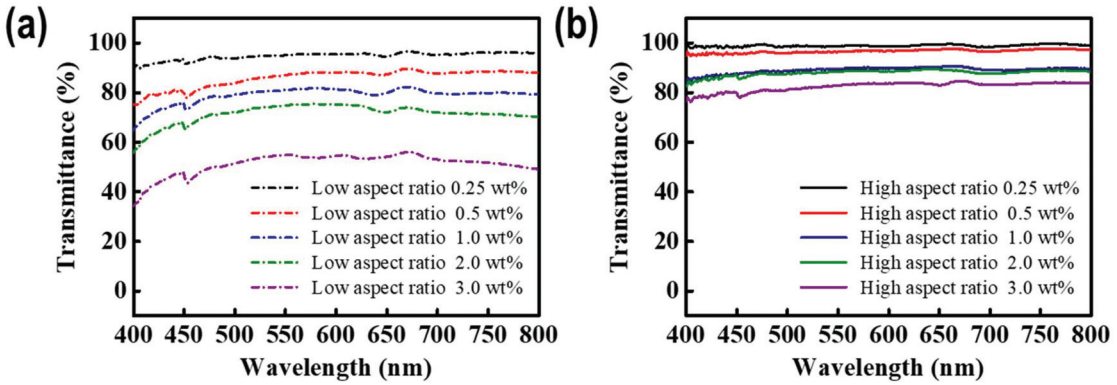

Fig. 4 Optical transmittance *versus* wavelength of the self-assembled AgNWs. (a) Low aspect ratio. (b) High aspect ratio.

transmittance is above 82% under all conditions. The reason for the high transmittance for the high aspect ratio is that the pattern is assembled with more open areas than that with the low aspect ratio for the same concentration of AgNWs. This can be confirmed by comparing the cell size distributions of the two types of AgNWs, as shown in Fig. S4.† With the same average diameter of 43.3–45.6 nm, the nanowires only differ in length: 30 μm on average for the low aspect ratio nanowires and 150 μm on average for the high aspect ratio nanowires. Among nanowires with the same flexural rigidity, longer nanowires produce wider curvatures[26] that determine the cell size. This phenomenon would be magnified when the nanowires floating on the solvent are arranged induced by the above-mentioned self-assembly, making robust use of the synergy of the migration control and the evaporation of solvents.

Compared to a conventional ITO film with haze values ranging from 1% to 3%,[27] AgNW electrodes suffer from high haze, or strong light scattering by the metal surface in the visible range. Typical AgNW electrodes have haze values in the range of 5%–15%,[28,29] and this is a major disadvantage that restricts the application of AgNWs in TEs. Thus, there is a real need to decrease the haze to the level of ITO films. The haze values of the well-connected AgNW patterns are measured using a haze meter; the results are shown in Fig. S5.† The haze value increases as the concentration of AgNWs increases, and it exceeds 5% as the silver concentration increases to 1.0 wt% because of the diffuse scattering. When the silver concentration is less than 1.0 wt%, the silver networks formed with low aspect ratio AgNWs showed a haze of 2.44% (0.25 wt% Ag), which increased slightly to 3.71% for 0.5 wt% Ag. The corresponding networks with low aspect ratio AgNWs exhibited a haze of 0.60% with 0.25 wt% Ag and 1.21% with 0.5 wt% Ag. At low AgNW concentrations, the high-aspect-ratio AgNW network exhibited a relatively low haze. It is regarded that the wider areas of cell-to-cell distance using the low aspect ratio AgNW cause a more extended silver domain, which leads to a larger amount of light scattering (see Table S1†).

Intense pulsed (IPL) sintering was used to treat the AgNW-patterned TE through a high-intensity flash of light (1000 kW for 2000 μs with a split number of 3) to decrease the sheet resistance (R_s) by facilitating rapid Ag-to-Ag sintering. As shown in Table 1, R_s decreases when power higher than 1000 kW is applied. However, distinct damage occurs not to the silver nanowires but to the surface of the substrate (PET) film, as shown in Fig. S6.† The bright domains, indicated by black arrows with ring boundaries, are exposed PET surfaces damaged by overheating. The dark domains surrounding the bright ring domains—indicated by white arrows—are the assembly of AgNWs that are randomly segregated; this leads to the disconnection of the silver networks. Therefore, IPL sintering should be performed only at intensities that do not damage the substrate. The split number of the IPL also the crucial factor to determine the low R_s, without spoiling the substrate surface. Thus, the optimum IPL conditions can be fixed by keeping the parameters under on- and off-times of 2000 μs, under 1000 kW of power, with a split number of 7. Under these conditions, we obtained the lowest R_s with no damage to the PET substrate. Fig. 5 shows the status of the silver nanowire junction using SEM images (Fig. 5a and b) and the variation in sheet resistance (see Fig. 5c, d, and Table S1†) as a function of AgNW concentration before and after IPL treatment. A fused silver junction is observed on the IPL-treated Ag networks, and it leads to a reduction in R_s.[30] Thus, IPL treatment is regarded to facilitate not only the rapid silver junction formation between the silver networks but also to promote the strong adhesion of metallic nanowires on flexible polymer substrates. As shown in Table S1,† the TE for the low aspect ratio AgNWs at 0.5 wt% exhibits similar transparency and R_s to the high aspect ratio AgNWs at 2.0 wt%; the SGAgNW patterns formed by the low aspect ratio AgNWs have a transmittance of 87.08% and R_s of 21.36 Ω $\square^{-1}$, while the high-aspect-ratio AgNWs have a transmittance of 88.42% and R_s of 25.44 Ω $\square^{-1}$.

The 550 nm transmittances for different concentrations of AgNW distributions formed on TE were compared for

Table 1 Intensive pulsed light sintering conditions for welding the AgNW junctions

#	On time	Off time	Power	Spilt number	R_b^*	R_a^*	ΔR_S^*	Damaged
1			1000 kW	1	52.64	52.20	0.44	
2	1000 μs	0 μs	1500 kW	1	52.55	48.53	4.02	
3			2000 kW	1	53.10	44.60	8.5	
4			1000 kW	1	52.8	50.54	2.26	
5	2000 μs	0 μs	1500 kW	1	52.65	42.72	9.93	
6			2000 kW	1	52.70	29.55	23.15	
7			1000 kW	3	52.88	38.63	14.25	
8	2000 μs	2000 μs	1500 kW	3	52.75	25.32	27.43	v
9			2000 kW	3	52.57	20.68	31.89	v
10				5	52.73	26.78	25.95	
11	2000 μs	2000 μs	1000 kW	7	52.67	21.36	31.31	
12				10	52.84	10.90	41.94	v

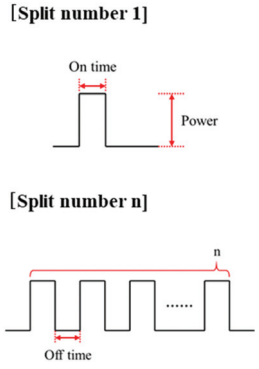

R_b: Sheet resistance before IPL sintering (ohm per sq.). R_a: Sheet resistance after IPL sintering (ohm per sq.). ΔR_s: Difference between R_b and R_a.

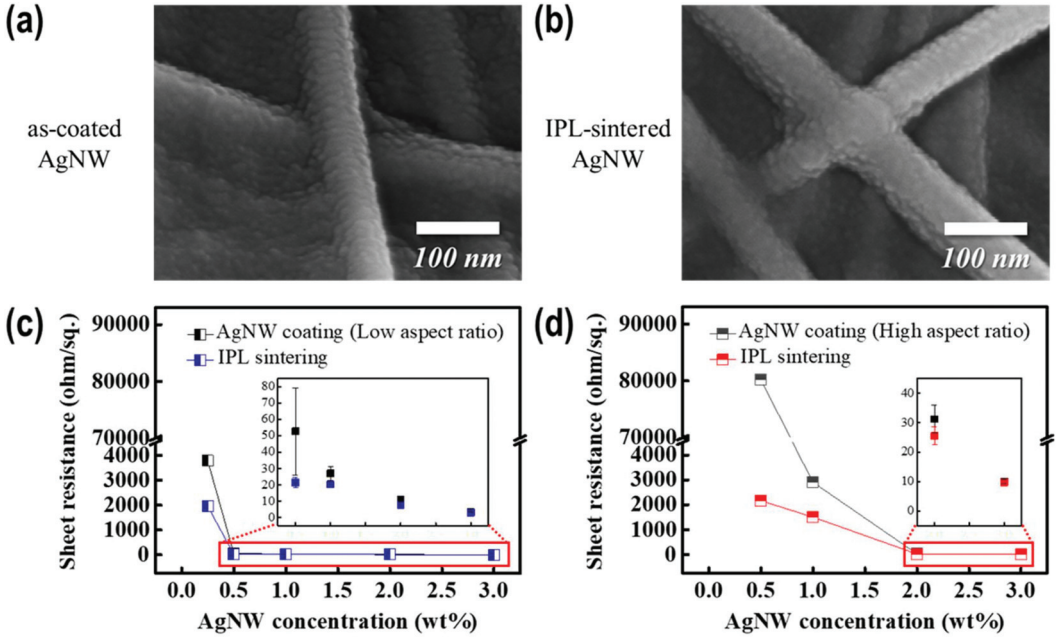

Fig. 5 Electrical properties of the self-assembled AgNW transparent electrodes. (a) SEM images of the as-coated electrode. (b) SEM images of the self-assembled electrode. (c) Sheet resistance for the low aspect ratio. (d) Sheet resistance for the high aspect ratio.

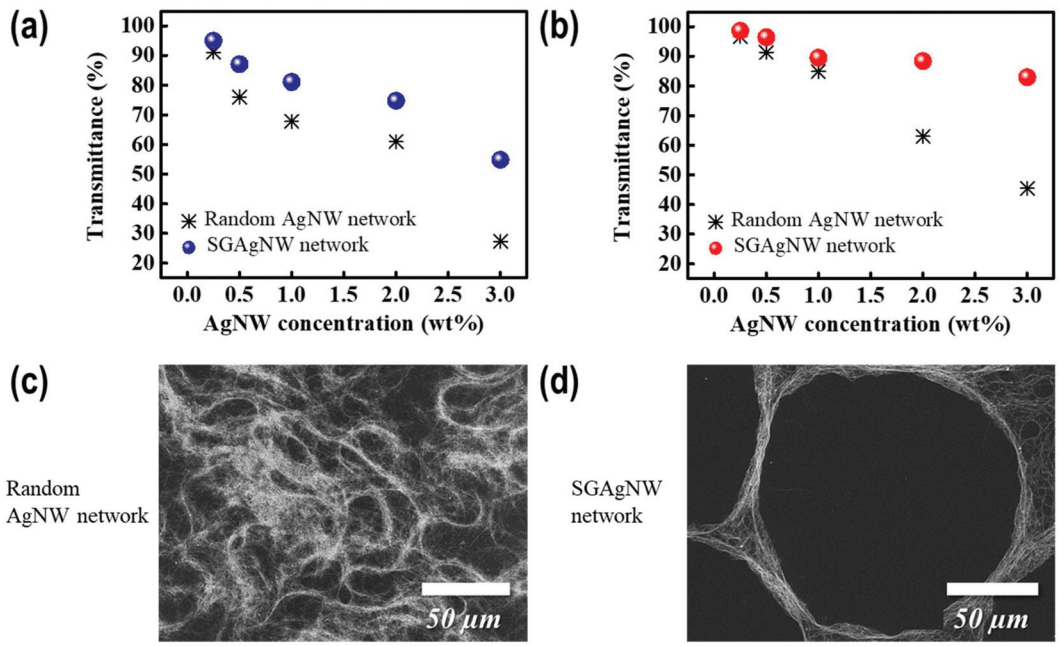

Fig. 6 Comparison of the random AgNW network and self-assembled AgNW network. (a) Optical transmittance at a wavelength of 550 nm for the low aspect ratio. (b) Optical transmittance at a wavelength of 550 nm for the high aspect ratio. (c) SEM image of the random AgNW network at 1.0 wt% for the low aspect ratio. (c) SEM image of the self-assembled AgNW network at 1.0 wt% for the low aspect ratio.

SGAgNWs and random patterns. The morphological differences were confirmed by the SEM images shown in Fig. 6. The film formed with the SGAgNW networks, without considering the aspect ratio, showed higher transmittance for each concentration than the corresponding film with random networks, even when no obvious morphological difference was observed in the SEM images (Fig. S7†). Furthermore, the silver nanowire networks were completely covered in the case of a randomly

distributed film, whereas the segregated silver nanowire networks with an empty space were formed surrounded by a conducting assembly of silver nanowires when the SGAgNW pattern was created. This verifies the superior properties of the segregated networks required for a TE device. The optoelectronic performance of a TE for each conductive material was compared by a figure of merit (FoM), which indicates the performance of the TE.[31] The optical and electrical properties of a transparent thin-film electrode can be compared using the following[31,32]:

$$T = \left(1 + \frac{Z_0}{2R_s}\frac{\sigma_{op}}{\sigma_{dc}}\right)^{-2} \quad (1)$$

$$\mathrm{FoM} = \frac{\sigma_{dc}}{\sigma_{op}} = \frac{Z_0}{2R_s(T^{-\frac{1}{2}} - 1)} \quad (2)$$

where σ_{dc}/σ_{op} denotes the ratio of the DC conductivity to the optical conductivity (here quoted at λ = 550 nm), R_s the sheet resistance, and Z_0 the impedance of free space (377 Ω). Compared with previous papers[15,33–37] that employed different coating methods, this template-free self-assembly coating method exhibits a superior FoM. The SGAgNW networks formed by low-and high-aspect-ratio AgNWs show FoMs of 123 and 117, respectively, which are higher than the previously reported FoM values (Table S2†). This confirms the utility of simple and cost-effective self-assembly over complex and expensive coating methods.

It is complicated to clarify the formation mechanism of the core–shell type SGAgNW network because solvent evaporation leads to the densification of the AgNW concentration and the redistribution of the AgNWs in the ink solution. When the ink solution is coated on the surface of the PET film that is heated on a hot plate by bar coating, the homogeneously distributed nanowires gradually form a segregated structure with interconnected metal patterns according to the solvent evaporation (Fig. 1 and 7). In previous studies,[38–40] ring-shaped self-assembled deposition techniques for a transparent conductive film were explained based on the ubiquitous coffee-ring effect, which is a capillary effect. The drop contact line remains fixed while the drying process begins; the suspended particles tend to gather at the drop edge because of the capillary outflow to replace the local rapid solvent loss at the drop edge.[41] However, this phenomenon coincides with the Marangoni effect, which is a surface capture effect and the preferential deposition of the solute at the center of a droplet caused by a recirculatory flow driven by the latent heat of evaporation that reverses the capillary effect.[42] Thus, the formation of the SGAgNW pattern (see Fig. 2 and S4†) confirms that the strong capillary outflow is dominant rather than a surface capture effect related to the rate of surface descent. The difference in deposition between the two types of AgNWs during the drying process is complex to explain using the above description. However, only SGAgNW patterns created by employing 0.5 and 1.0 wt% Ag (concentrations optimized for their practical

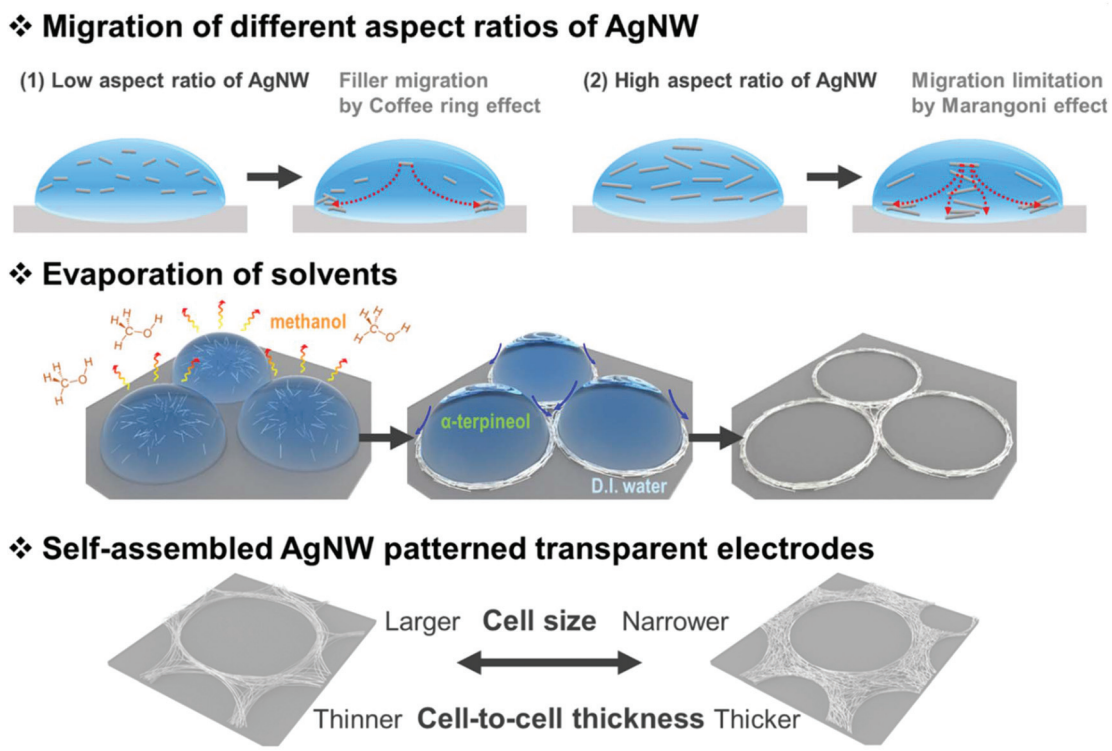

Fig. 7 Schematic of the self-assembly of AgNW networks.

optical properties) were dominantly influenced by the coffee-ring effect over the Marangoni effect during the formation of the segregated pattern (Fig. 7). The filler movement in the case of a high aspect ratio was relatively restricted by the Marangoni effect, which resulted in a smaller cell size. Thus, the shape of the pattern can be changed according to the aspect ratio of the metal NWs, which enables the control of the TE transmittance. (See Table S1,† where the average cell size of the patterns formed by the low aspect ratio Ag is wider than that of others.)

In a water-based silver ink solution, instead of the Marangoni effect-based cell pattern (T = 70 °C), a coffee-ring effect based cell structure pattern is normally obtained at a lower temperature (T = 30 °C) to slow the surface evaporation.[41] This capillary flow based deposition during the drying process could be enhanced by a combination of solvents: methanol, α-terpineol, and DI water. Alpha-terpineol has a hydrophobic property with high viscosity (67 mPa s), notably higher than that of water (1.001 mPa s), and a high boiling point (220 °C) (Table S3† contains information on the solvent properties). Because of these properties, it is used as an organic vehicle to suspend silver nanoparticles, while preventing sedimentation on the silver paste,[43] and it is used to regulate the solvent volatility in the preparation of silver screen-printing ink.[44] During the heating process, the surface level of the as-coated silver ink solution on the surface-treated PET film began to descend by evaporation of methanol at 70 °C. Because α-terpineol has high viscosity and is insoluble in DI water, the solution after methanol evaporation leaves small α-terpineol droplets that are distributed separately from the water. The hydrophilic AgNW particles contained in the water remain in the water matrix, while the water drops were ousted to the edges of the terpineol droplets because the hydrophobic property of α-terpineol leads to the formation of a densified AgNW network with a segregated structure. The SGAgNW structure was further densified during the second step of the heat treatment at 135 °C. Afterward, a filler-to-filler junction was created through IPL treatment with the complete removal of the organic solvent.

The SGAgNW-based thin film was applied as a transparent film heater to envisage its potential as a flexible TE (see Fig. S8–11† for the results and descriptions in the ESI†). The SGAgNW-based thin film with high transparency showed a stable heating performance under the application of DC voltage from 1 V to 10 V, and the heat could be controlled from 34.5 °C to 94.5 °C in accordance with the applied DC voltage. A short response time of less than 3 min was observed to achieve the saturated temperature (T_{80}: 80% of the saturated response) under all conditions while maintaining a stable temperature. Furthermore, during five heating and cooling cycles under a DC voltage of 7 V, the TE film heated to an average of 61.3 °C ± 0.6 °C with a narrow deviation; this confirmed the reliability and thermal stability of the transparent thin film heaters.

Thus, the proposed technique based on the present solution-based coating process can be applied to design transparent conductive patterns. These patterns are deposited selectively on specific areas with desired morphologies for their applications in flexible optoelectronics such as wearable displays, smart windows, electrochromic films, flexible transparent film heaters, and photovoltaic panels.

Conclusions

The segregation-based self-assembly of silver nanowire networks for fabricating transparent thin-film electrodes was demonstrated by patterning structure-controlled groups of AgNWs on a polyethylene terephthalate substrate using a template-free solution-based process. Open areas in the silver network with a typical cell size of less than 350 μm were located at the center of the pattern; these areas contributed to the high transparency of the film and the consecutively connected silver assembly led to the enhancement of the electrical conductivity. The morphology of the pattern could be tuned by adjusting the concentration and aspect ratio of the metal nanowires. When two types of AgNWs with different aspect ratios were compared, a low aspect ratio (L/D ~1000) was found to be more effective in forming uniform spherical patterns exhibiting a high optical transmittance of 87.08% and low Rs of ~50 Ω □$^{-1}$ at a concentration of 0.5 wt% of the nanowires; this could then be further reduced to 21.36 Ω □$^{-1}$ by creating wire-to-wire junctions using IPL treatment. The film with the SGAgNWs was identified to have a superior haze value of less than 3.71% compared with AgNWs with a high aspect ratio (~3000) that have haze values exceeding 6.40%; it showed similar optical and electrical properties (88.42% transmittance and R_s ~25.44 Ω □$^{-1}$) to 2.0 wt% AgNWs. The SGAgNWs were formulated *via* the migration control of AgNWs with different aspect ratios coupled with the tailored evaporation of solvents with different viscosities, vapor pressures, and solubilities. This SGAgNW-based technology is a cost-effective coating technology that uses the self-assembly of a well-connected AgNW network. This technology has promising potential for use as a TE device in next-generation optoelectronics.

Conflicts of interest

There are no conflicts to declare.

Acknowledgements

This work was supported by a National Research Foundation of Korea (NRF) grant funded by the Korean government (MSIT) (no. 2015R1A5A1037548), the Nanomaterial Technology Development Program through the NRF funded by the Ministry of Science, ICT and Future Planning (no. 2016M3A7B4900044), and the Future Materials Discovery Program through the NRF funded by the Ministry of Science, ICT & Future Planning (NRF-2019M3D1A210415).

References

1 H.-G. Cheong, D.-W. Song and J.-W. Park, *Microelectron. Eng.*, 2015, **146**, 11–18.
2 S. Hong, H. Lee, J. Lee, J. Kwon, S. Han, Y. D. Suh, H. Cho, J. Shin, J. Yeo and S. H. Ko, *Adv. Mater.*, 2015, **27**, 4744–4751.
3 P.-H. Wang, S.-P. Chen, C.-H. Su and Y.-C. Liao, *RSC Adv.*, 2015, **5**, 98412–98418.
4 D. S. Hecht, L. Hu and G. Irvin, *Adv. Mater.*, 2011, **23**, 1482–1513.
5 H. Peelaers, E. Kioupakis and C. G. Van de Walle, *Appl. Phys. Lett.*, 2019, **115**, 082105.
6 D. Langley, G. Giusti, C. Mayousse, C. Celle, D. Bellet and J.-P. Simonato, *Nanotechnology*, 2013, **24**, 452001.
7 J. A. Rogers, T. Someya and Y. Huang, *Science*, 2010, **327**, 1603–1607.
8 M.-C. Choi, Y. Kim and C.-S. Ha, *Prog. Polym. Sci.*, 2008, **33**, 581–630.
9 Y. Ishikawa and M. B. Schubert, *Jpn. J. Appl. Phys.*, 2006, **45**, 6812–6822.
10 M. l. Lagrange, D. P. Langley, G. Giusti, C. Jiménez, Y. J. M. Bréchet and D. Bellet, *Nanoscale*, 2015, **7**(41), 17410–17423.
11 G.-C. He, H. Lu, X.-Z. Dong, Y.-L. Zhang, J. Liu, C.-Q. Xie and Z.-S. Zhao, *RSC Adv.*, 2018, **8**, 24893–24899.
12 P. Zhang, I. Wyman, J. Hu, S. Lin, Z. Zhong, Y. Tu, Z. Huang and Y. Wei, *Mater. Sci. Eng., B*, 2017, **223**, 1–23.
13 A. F. Harper, P. J. Diemer and O. D. Jurchescu, *npj Flex. Electron.*, 2019, **3**, 11.
14 X. Bai, S. Lin, H. Wang, Y. Zong, H. Wang, Z. Huang, D. Li, C. Wang and H. Wu, *npj Flex. Elec*, 2018, **2**, 3.
15 J. H. M. Maurer, L. Gonzalez-Garcia, B. Reiser, I. Kanelidis and T. Kraus, *Nano Lett.*, 2016, **16**, 2921–2925.
16 J. M. Gaskell and D. W. Sheel, *Thin Solid Films*, 2012, **520**, 4110–4113.
17 T. Kim, A. Canlier, G. H. Kim, J. Choi, M. Park and S. M. Han, *ACS Appl. Mater. Interfaces*, 2013, **5**, 788–794.
18 S. Liu, B. Sun, J.-g. Li and J. Chen, *CrystEngComm*, 2014, **16**, 244–251.
19 Y. Sun, Y. Ren, Y. Liu, J. Wen, J. S. Okasinski and D. J. Miller, *Nat. Commun.*, 2012, **3**, 971.
20 Y.-R. Jang, S.-J. Joo, J.-H. Chu, H.-J. Uhm, J.-W. Park, C.-H. Ryu, M.-H. Yu and H.-S. Kim, *Int. J. Precis. Eng.*, 2021, **8**, 327–363.
21 M. Dexter, A. Pfau, Z. Gao, G. S. Herman, C.-h. Chang and R. Malhotra, *Nanotechnology*, 2018, **29**, 505205.
22 C.-J. Lee, D.-G. Kang, B.-U. Hwang, K. D. Min, J. Joo and S.-B. Jung, *J. Alloys Compd.*, 2021, **863**, 158726.
23 S. Haghanifar, R. T. Rodriguez De Vecchis, K.-J. Kim, J. Wuenschell, S. P. Sharma, P. Lu, P. Ohodnicki and P. W. Leu, *Nanotechnology*, 2018, **29**, 42LT01.
24 M. Shahpanah, S. Mehrabian, M. Abbasi-Firouzjah and B. Shokri, *Surf. Coat. Technol.*, 2019, **358**, 91–97.
25 I. Junkar, A. Vesel, U. Cvelbar, M. Mozetič and S. Strnad, *Vacuum*, 2009, **84**, 83–85.
26 A. Vazinishayan, S. Yang, D. R. Lambada and Y. Wang, *Results Phys.*, 2018, **9**, 218–224.
27 L. B. Hu, H. S. Kim, J. Y. Lee, P. Peumans and Y. Cui, *ACS Nano*, 2010, **4**, 2955–2963.
28 A. Hubarevich, M. Marus, Y. Mukha, K. Wang, A. Smirnov and X. W. Sun, *AIP Adv.*, 2019, **9**, 045226.
29 M. Marus, A. Hubarevich, W. J. Fan, H. Wang, A. Smirnov, K. Wang, H. Huang and X. W. Sun, *AIP Adv.*, 2018, **8**, 035201.
30 J. Jiu, T. Sugahara, M. Nogi, T. Araki, K. Suganuma, H. Uchida and K. Shinozaki, *Nanoscale*, 2013, **5**, 11820–11828.
31 S. De, T. M. Higgins, P. E. Lyons, E. M. Doherty, P. N. Nirmalraj, W. J. Blau, J. J. Boland and J. N. Coleman, *ACS Nano*, 2009, **3**, 1767–1774.
32 C. Zhang and V. Nicolosi, in *2D Metal Carbides and Nitrides (MXenes): Structure, Properties and Applications*, ed. B. Anasori and Y. Gogotsi, Springer International Publishing, Cham, 2019, pp. 481–501.
33 S. Wu, L. Li, H. Xue, K. Liu, Q. Fan, G. Bai and J. Wang, *ACS Nano*, 2017, **11**, 9898–9905.
34 S. Gong, Y. Zhao, L. W. Yap, Q. Shi, Y. Wang, J. A. P. B. Bay, D. T. H. Lai, H. Uddin and W. Cheng, *Adv. Electron. Mater.*, 2016, **2**, 1600121.
35 Y. D. Suh, S. Hong, J. Lee, H. Lee, S. Jung, J. Kwon, H. Moon, P. Won, J. Shin, J. Yeo and S. H. Ko, *RSC Adv.*, 2016, **6**, 57434–57440.
36 S. Ahn, A. Choe, J. Park, H. Kim, J. G. Son, S.-S. Lee, M. Park and H. Ko, *J. Mater. Chem. C*, 2015, **3**, 2319–2325.
37 S. Hong, J. Yeo, G. Kim, D. Kim, H. Lee, J. Kwon, H. Lee, P. Lee and S. H. Ko, *ACS Nano*, 2013, **7**, 5024–5031.
38 D. Mampallil and H. B. Eral, *Adv. Colloid Interface Sci.*, 2018, **252**, 38–54.
39 A. Shimoni, S. Azoubel and S. Magdassi, *Nanoscale*, 2014, **6**, 11084–11089.
40 C. Seo, D. Jang, J. Chae and S. Shin, *Sci. Rep.*, 2017, **7**, 500–500.
41 Y. Li, Q. Yang, M. Li and Y. Song, *Sci. Rep.*, 2016, **6**, 24628.
42 H. Hu and R. G. Larson, *J. Phys. Chem. B*, 2006, **110**, 7090–7094.
43 H. Z. Li, Z. Xiaoyang, L. Zhenghao, Y. Jianjun and L. Hongbo, *Nanomaterials*, 2020, **10**, 107/101–107/107.
44 W. Yuan, X. Wu, W. Gu, J. Lin and Z. Cui, *J. Semicond.*, 2018, **39**, 015002.

